Use of Aqueous Solutions to Simulate Supercritical CO_2 Corrosion

S. Sim,[‡,,**] P. Corrigan,[**] I.S. Cole,[**] and N. Birbilis[*]*

ABSTRACT

Capturing and storage of anthropogenic carbon dioxide (CO_2) requires the transport of CO_2 with varying combinations of impurities depending on the capture technology and source. Traditional pipelines are not designed for the transport of such relatively low-purity CO_2; in fact, initial research indicates that a low-purity CO_2 environment poses a significant durability risk to conventional (gas) pipelines. The presence of water in a supercritical CO_2 stream will lead to acidic conditions via the formation of carbonic acid (H_2CO_3). In this work, a round robin of experiments has been executed in aqueous solutions where CO_2 has been added to water to form H_2CO_3 in situ, along with testing in sulfuric acid (H_2SO_4) that was found to simulate the impact of H_2CO_3 upon steel. The role of Cl^-, NO_3^-, and SO_4^{2-} impurities was also investigated. Conclusions have been drawn from electrochemical, weight-loss, and optical profilometry results, with future work outlined. While not a replacement to supercritical CO_2 experiments, we see that there is significant merit in such high throughput tests to form an initial understanding, which can be subsequently benchmarked by supercritical CO_2 tests.

KEY WORDS: carbonic, carbon capture and storage, carbon dioxide, corrosion, pipeline, supercritical, sulfuric acid

INTRODUCTION

Transport of supercritical carbon dioxide (CO_2) from capture locations to storage locations will require cost-effective and durable pipelines. However, to date, little is known about the corrosion behavior of steel in the presence of CO_2 streams that are typical of those used in carbon capture and storage (CCS). A simplified diagram of the CCS process is presented in Figure 1.

Although CO_2 corrosion of pipelines used in oil and gas industries has been studied widely in the last few decades,[1-4] in those instances, CO_2 is an impurity in the stream, not the main component as in CCS. Further, CCS pipelines will operate at significantly higher pressures so that care must be taken in translating information from oil and gas transport to CCS. The transport of CO_2 by pipelines in enhanced oil recovery (EOR) systems, however, sees operation under similar pressures and temperatures to that which will be used in CCS. There are currently ~3,100 miles (~5,000 km) of EOR-CO_2 pipeline in existence in the United States. The EOR-CO_2 pipelines have been operating for up to 20 years with no significant record of corrosion. Such pipelines are operated under strict limitations on contaminants, particularly free water, hydrogen sulfide (H_2S), S compounds, and oxygen.[5]

The area of CCS has only started to gain support in terms of development and implementation over the last decade (compared to renewable energy which has been researched since the 1970s) because of the environmental risks associated with high CO_2 emissions[6] (global warming, etc.). In a recent paper by Goodman, et al., the United States Department of Energy (U.S. DOE) has developed a methodology for estimating CO_2 storage potential for oil and gas reserves and saline formations[7] ("geological storage" step in Fig-

Submitted for publication August 18, 2011.
‡ Corresponding author. E-mail yeat.sim@monash.edu.
* Department of Materials Engineering, Monash University, Clayton, Victoria 3800, Australia.
** CSIRO Materials Science and Engineering, Private Bag 33, Clayton South, Victoria 3169, Australia.

ISSN 0010-9312 (print), 1938-159X (online)
12/000063/$5.00+$0.50/0

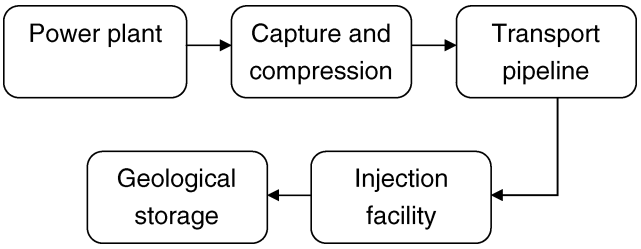

FIGURE 1. *Simplified diagram of CCS process.*

TABLE 1
Possible CO_2-Rich Gas Composition from Post-Combustion, Pre-Combustion, and Oxyfuel Capture Based on a Coal-Fired Power Station[13]

Component	Post-Combustion (vol%)	Pre-Combustion (vol%)	Oxyfuel (vol%)
CO_2	99.97	96.39	95.80
CH_4	—	0.01	
N_2	0.0033	0.2	1.23
H_2S	—	0.6	—
C_2^+	—	—	—
CO	—	0.4	—
O_2	0.0033	0.2	1.23
NO_x	0.01	—	0.01
SO_x	0.01	—	0.5
H_2	—	2.0	—
Ar	0.0033	0.2	1.23

ure 1). Their interest in this area shows the continued advancement of CCS despite knowledge gaps in the transportation phase associated with supercritical CO_2 and potential impurities.

The reasons for the need to take care when translating experience in oil and gas transport to CCS are two-fold. First, the precise chemical nature of the streams remains unknown and will vary depending on the nature of the source (i.e., combustion of fossil fuel—coal, oil and gas in power plants, and industrial processes such as mineral or metal production). Second, CO_2 from CCS is destined to be transported most economically as a supercritical fluid (>7.38 MPa [or 70 bar] at about 31.1°C)[8] because of its high density and to avoid complicated two-phase (gas + liquid) flow regimes and pressure drop.[9] As such, determination of actual corrosion kinetics in such conditions is not trivial, since the CCS pipeline pressure is more than 3 times greater than that used for oil and gas. Only recently has experimental data collection been attempted and reported,[10-12] where a limited but critical data set will emerge in coming years.

As seen in Figure 1, capture and compression of CO_2 precedes the transportation phase, hence determining CO_2 stream composition. Table 1 gives an approximation of the stream composition based on the three primary capture technologies—post-combustion, pre-combustion, and oxyfuel. The source of CO_2 for all three technologies is from coal-fired power stations.

From Table 1, this compilation of data shows that post-combustion yields the highest percentage of CO_2 at 99.97% purity. All three processes are able to yield high-purity CO_2, but are held back by the same technical difficulty—the challenge of limiting NO_x and SO_x impurities. In recent months, the oxyfuel process has been discussed widely as being one of the most promising processes for CCS, with research focused on reducing NO_x and SO_x by using flue gas cleaning systems.[14]

In a study by Ayello, et al., electrochemical impedance spectroscopy (EIS) results revealed detrimental effects from the addition of low volumes of impurities (1 mM hydrochloric acid [HCl], 1 mM nitric acid [HNO_3]) to a 1,000 ppm CO_2-H_2O solution. Corrosion rates increased from 0.1 mm/y to 5.6 mm/y with HCl and 4.5 mm/y with HNO_3. This was believed to be attributed to a low dilution factor when water levels are low. Thermodynamic modeling also revealed that higher volumes (0.5 M to 1 M) of impurities would further increase corrosion rates, though there is still limited knowledge on the chemical reactions that potentially could occur.[12] Subsequently, experimental tests in this paper aim to fill this knowledge gap by providing corrosion rates of Cl^-, NO_3^-, and SO_4^{2-} impurities in a similar acidic environment.

In a recent review by Cole, et al.,[5] four regimes with different risks of corrosion were outlined for supercritical CO_2 transport.

Very Low Contaminant Levels and Extremely Low Water Content

In this regime, corrosion damage is minimal or nonexistent. It contains very low contaminant levels and extremely low water content. In a laboratory study conducted by McGrail, et al.,[15] it was indicated that approximately 600 ppmw is the critical value for water content from which corrosion will occur. This concurs with the EOR-CO_2 transport limit of 600 ppmw. However, this is in contrast with the work of Ayello, et al.,[10] who found significant corrosion at 100 ppmw.

Low Contaminant Levels and Water Content Below the Solubility Limit

In this regime, contaminant levels are low but water content has exceeded the critical value. Corrosion starts to take place at 0.38 mm/y[16] in the absence of impurities. However, at this stage, water content is still below the solubility limit so a separate phase does not occur.

Low-Moderate Contaminant Levels and Water Content Above the Solubility Limit

In these regimes, the solubility limit of water in CO_2 has been exceeded, resulting in a separate phase. The difference between these two regimes is the increased concentration of impurities, where they

tend to segregate into the aqueous phase containing CO_2, carbonic acid (H_2CO_3), and water.

The purity of the gas stream is controlled by pollutant control measures at the power plant or other sources of CO_2, by the effect of CO_2 capture and gas conditioning prior to piping the gas. The first regime is typical of CO_2 transport in EOR in the USA (under Kinder Morgan guidelines[5]) and would prevail if CO_2 were extracted using monoethanolamine (MEA) in a plant with strong pollution control measures and gas conditioning to lower the water content below the pressure solubility limit (500 ppm in CO_2). The second regime would occur if gas conditioning was limited or there was a limited source of H_2O in the pipe. The third could occur in the absence of gas conditioning, or with additional sources of H_2O, while the fourth would occur without gas conditioning and limited cleaning of the gas at source.

In the CCS process, potential damage may occur to ferrous pipelines when the CO_2 stream is contaminated by free water (H_2O),[15,17] resulting in the in situ formation of H_2CO_3. A relatively high acid concentration may evolve, owing to the high operating pressure, which allows a (relatively) high solubility of CO_2 in water.[18] Empirical evidence suggests that corrosion rates can increase by two times (1.2 mm/y to 2.5 mm/y) when water concentration is increased (100 ppm to 2,000 ppm).[10] The in situ speciation of H_2CO_3 in the aqueous phase leads to the generation of low pH, ~3.2, as determined by Ayello, et al.,[10] via experiments and simulation.[19] This is an environment that is aggressive and detrimental to carbon steels including mild and X-60/65/70/80 grades. Experiments have shown that carbonate ($FeCO_3$) layers can form on a steel surface, which is susceptible (as a result of the instability of the layer) to corrosion in acidic solutions.[18] Despite this, ferrous metals are essentially the only viable candidate for CCS pipelines based on the operating pressure of such pipelines. Another concern is pressure drop in pipelines that occur because of frictional forces, thus reducing the solubility of water in the CO_2 phase, which could lead to the formation of an aqueous phase.[20]

To date, experimental and theoretical works have found that the lowest pH attributed from H_2CO_3 alone is about 3.2.[5] In addition, the aggressive nature of impurities such as sulfates (SO_x), nitrates (NO_x), and chlorides (Cl^-) from capture technologies[21-23] can cause an additional, and presently uncharacterized, durability threat. Current capture technologies include absorption, adsorption, and membrane and cryogenic processes, of which chemical absorption via solvents (i.e., MEA) will be the most likely candidate for commercial purposes.[24] In a water-CO_2 system, these impurities tend to segregate into the aqueous phase, which can potentially drop the pH further by the in situ formation of sulfuric acid (H_2SO_4) and nitric acid (HNO_3) (in addition to the existing H_2CO_3). Experimental work has shown that corrosion rates are four times greater (than in pure supercritical CO_2) when trace levels of HCl and HNO_3 impurities are added in supercritical CO_2 with an aqueous phase, despite no changes in water solubility limit.[10]

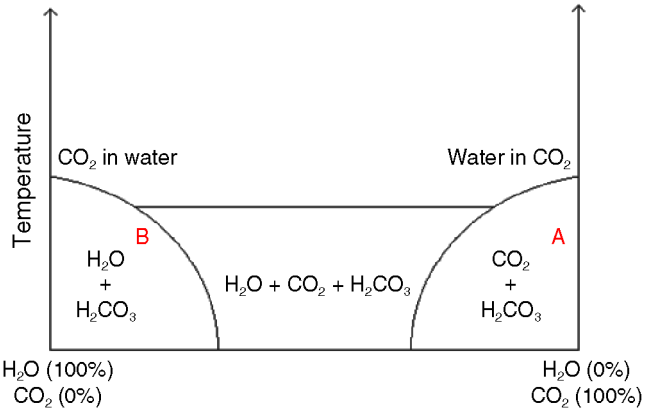

FIGURE 2. *Simplified phase diagram of the water-CO_2 system (from left to right), showing CO_2 in water (100% H_2O + H_2CO_3), an aqueous region containing H_2O and CO_2 with H_2CO_3 in H_2O, and water in CO_2 (100% CO_2 + H_2CO_3).*

At present, no construction or operation standards for CCS pipeline transportation have been developed at the national level; however, while there is now much activity in this area,[7] there remains insufficient benchmark data for both the stream chemistry and corrosion rates achieved in the presence of H_2CO_3 to understand fully the extent of damage from supercritical CO_2 corrosion. To begin to understand the amount of damage accumulated in such environments, the goal of this study was to use environments that may begin to simulate the aqueous phase in impure supercritical CO_2 by the use of simulants (CO_2 in water, alternate acid, and impurities), on the premise/hypothesis that corrosion damage is dictated by acid strength (and subsequently the concentration of H_2CO_3 in practice). To rationalize the hypothesis, Figure 2 shows a schematic simplified phase diagram for the water-CO_2 system.

What can be seen from Figure 2 is that there are conceivably three phase fields (simplified by neglecting pressure and intermediate phases). The phase that poses the corrosion risk is H_2CO_3. The existence of H_2CO_3 in the CO_2 stream as a result of trace levels of water in CO_2 is indicated by point A. The existence of H_2CO_3 in water is indicated by point B, suggesting that a given concentration of H_2CO_3 can be achieved in conditions that readily allow the kinetics of corrosion to be measured.

Consequently, in this paper, we standardized the electrolyte nomenclature according to the concentration of H_2CO_3 present (to allow a pressure-independent parameter to be established for which data in supercritical CO_2 conditions ultimately can be com-

pared), along with the solution pH that arises for a given H_2CO_3 concentration. We additionally studied the impact of some common impurities in the context of corrosion rates measured electrochemically, and damage accumulation (profilometry, weight loss, and thickness loss). The environment of the experimental tests herein mimics conditions relative to regime four, where gas conditioning and cleaning of the gas at the source is very limited or non-existent.

This work will form part of a baseline for corrosion rates in supercritical CO_2 systems in a high throughput manner (owing to the use of aqueous electrolytes), and be particularly useful when calibrated with high-pressure data in follow-up experiments (which is inherently a low throughput methodology).

EXPERIMENTAL PROCEDURES

Four different tests were conducted to quantify corrosion in the presence of acid electrolytes in the laboratory setting. Potentiodynamic polarization tests were conducted to reveal kinetic and mechanistic aspects related to electrochemical processes; weight-loss and thickness loss tests were able to give a ground truth/cumulative representation of corrosion; finally, optical profilometry was able to reveal corrosion mode in regard to where there was pitting, etc., in addition to quantifiable damage statistics.

Experimental Procedures for Electrochemical Tests in Carbonic Acid Environments

Since H_2CO_3 only exists in solution, water was routinely carbonated in-house via high-pressure CO_2 injection (using compressed CO_2 and a Soda Stream[†] apparatus). In all cases, Melbourne (Australia) tap water was used to serve as a better simulant to impure water than distilled H_2O would. As the pH of solutions containing H_2CO_3 increases over time in the open environment (i.e., carbonation), their pH was measured with an electronic pH meter before and after the experiments to ensure accuracy. Ideally, the idea of the experiment was to obtain results in solutions that ranged from low to high pH, corresponding with various concentrations of H_2CO_3. However, since atmospheric pressure was used in these experiments, a range from pH 3.5 to ~7 was obtained. The pH was increased from 3.5 to desired levels by addition of water while monitoring with the pH meter. The minimum pH achieved of 3.5 is not too dissimilar to the theoretical pH achieved at higher pressures as reported by Choi and Nešić.[18] However, in this work, to expand the range of pH of the test solutions, additional tests were undertaken to gain results over a wider (i.e., lower) pH range (pH 1 to 7), using solutions prepared with H_2SO_4 to simulate the concentrated acidic environment present in supercritical CO_2 conditions. The samples used for testing were carbon steel (UNS G15256) sheet (0.22% to 0.29% carbon), with a surface preparation of 1200 grit silicon carbide (SiC) paper.

Electrochemical tests were conducted using a Biologic SP-50[†] potentiostat and a purpose-built three-electrode "flat cell." The cell consisted of a plastic vessel with cut-outs to accommodate 1 cm^2 of sample exposure to the electrolyte (carbonated water), as well as the reference and counter electrodes. The reference electrode used was a saturated calomel electrode, while a titanium mesh electrode (approximately 2 cm by 7 cm) was used as the counter electrode. A Luggin probe was not required for these experiments. Three sets of experiments were conducted at every ~0.5 pH increment with 100 mL of respective test solution, where all experiments were done in quiescent conditions. The cell had cut-outs to allow injection of CO_2 as needed, and a cut-out to allow continual pH monitoring. Under the control of EC-Lab,[†] experiments began with an open-circuit potential (OCP) exposure of 10 min followed by a potentiodynamic scan (PDS) at a scan rate of 1 mV/s.

Experimental Procedures for Long-Term Tests Including Weight Loss and Optical Profilometry

Steel samples with an approximate size of 1 cm by 1 cm were prepared. Samples then were divided into groups depending on the intended exposure, with each having 3 sets. Before experiments commenced, surface preparation included grinding to 1200 grit SiC paper under ethanol. Sample dimensions were measured with digital calipers and then weighed with a digital balance to 4 decimal places (of grams). Immersion time was 1 week in all cases.

After carefully removing the samples from the exposure beakers, any corrosion product was removed by a slight brushing following a 10 s agitation in a dilute HNO_3 solution. They then were measured with the digital calipers and balanced again to quantify changes in dimension and weight loss that occurred. Surface analysis was also conducted on these samples using a Veeco Wyko NT1100[†] optical profilometer. Each surface was sampled 3 times at random locations; and output from profilometry analysis was used to quantify pit depths and density upon the samples.

RESULTS AND DISCUSSION

Polarization Test Results Analysis

Example Polarization Curves — Rather than present large amounts of raw polarization data, typical plots are seen in Figure 3.

Figure 3 reveals that increases in corrosion rate associated with acidic electrolytes are largely governed by increases in the rate of the anodic reaction. As pH decreases from 7 (potable water) to 1 (H_2SO_4), the

[†] Trade name.

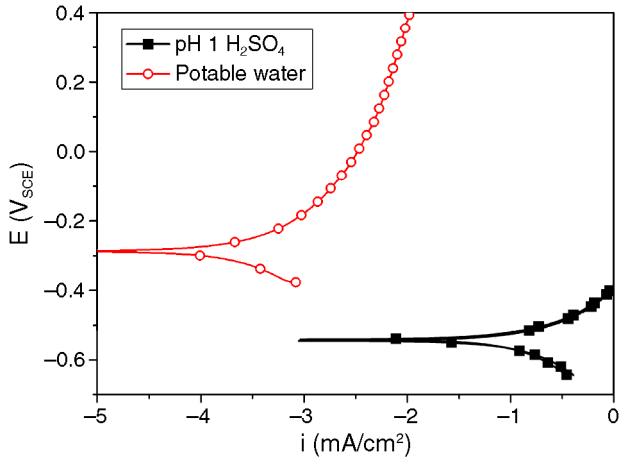

FIGURE 3. *Example of a potentiodynamic polarization curve of steel samples immersed in potable water and pH 1 H_2SO_4.*

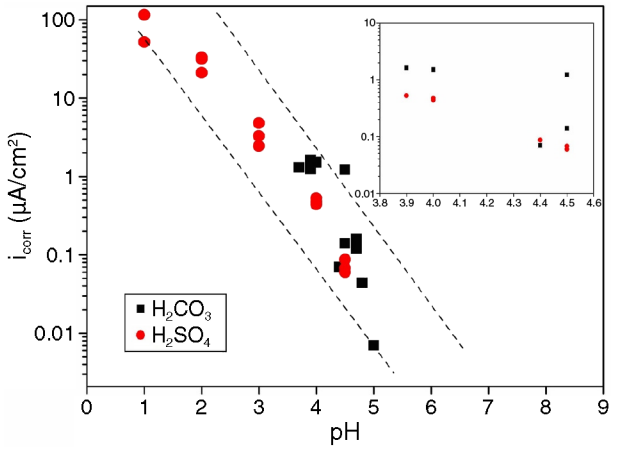

FIGURE 4. *i_{corr} vs. pH for tests conducted on steel samples in H_2CO_3 and H_2SO_4 at 25°C.*

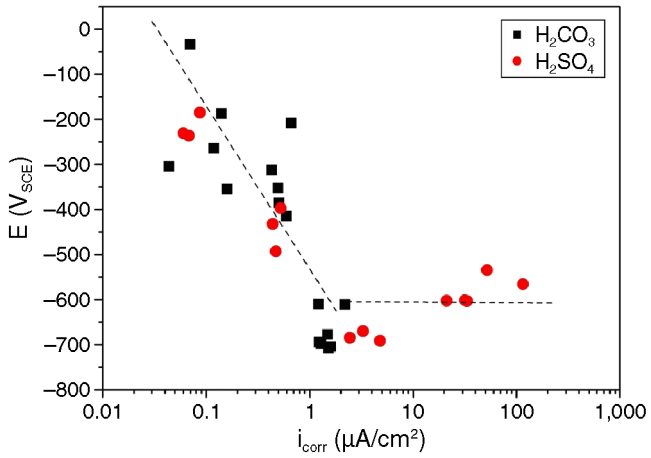

FIGURE 5. *E vs. i_{corr} for tests conducted on steel samples in H_2CO_3 and H_2SO_4 at 25°C.*

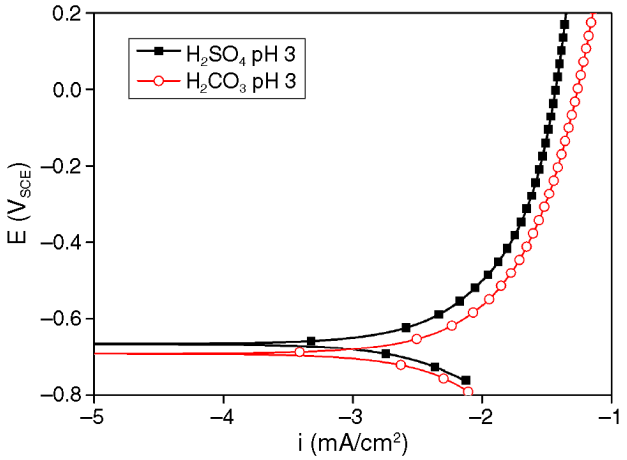

FIGURE 6. *Potentiodynamic polarization curves collected for steel samples in H_2SO_4 and H_2CO_3 adjusted to pH 3, 25°C.*

polarization curve shifts toward higher current values, indicating a marked increase in corrosion rate.

Polarization Response in Carbonic and Sulfuric Acids — Tafel extrapolation was performed on the polarization data collected in H_2CO_3-containing electrolytes and H_2SO_4 electrolytes (over a range of concentrations of both acids) to obtain their corrosion potential (E_{corr}) and corrosion current density (i_{corr}) values. As a result, abridged plots are constructed from the data obtained. Figure 4 shows the overall results of the H_2CO_3 and H_2SO_4 tests over the range of acidic pH. A further magnified version of the graph, which focuses on similar pH values (3.9 to 4.5) for both data sets, is also shown (Figure 4 inset).

The polarization response in both acids showed similar behavior, indicating that the corrosion mechanics (under acidic conditions) are largely pH-driven, independent of the chemistry between the acids. To show that similar mechanistic behavior occurs, a plot was made (Figure 5) of the E_{corr} vs. i_{corr} values, which revealed the trend is anodically driven (i.e., decreasing E_{corr} with increasing i_{corr}) and holds between the two acids, until a critical E_{corr} is reached.

As a further example, there is also very little difference between the polarization response when comparing the polarization curve in both acids adjusted to the same pH. This is seen in Figure 6.

The data on the basis of acid concentration are depicted in Figure 7.

It can be observed that both acids display a similar relationship, in which an increase in concentration increases the corrosion rate (Figure 7). However, it can be seen that H_2SO_4 is ~100 times (i.e., 2 orders of magnitude) more corrosive compared to H_2CO_3 on a concentration basis (not pH basis), which is synonymous with H_2CO_3 being a comparatively "weak" acid. This has immediate implications, as discussed below, in that should other "stronger" acids be able to speciate in situ owing to impurities, even low concentrations could amplify corrosion disproportionately.

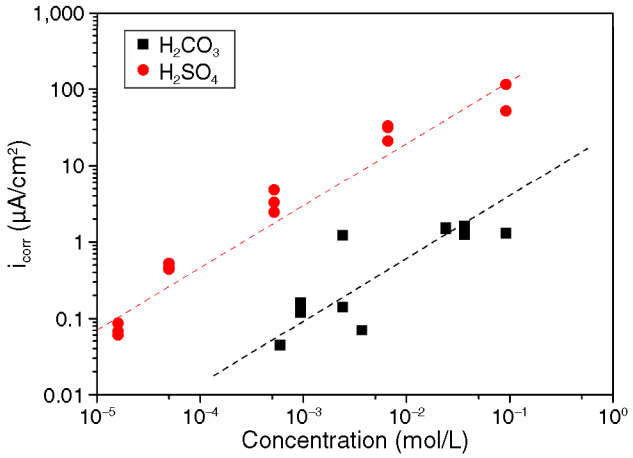

FIGURE 7. *i_{corr} vs. concentration of steel samples in H_2CO_3 and H_2SO_4 at 25°C.*

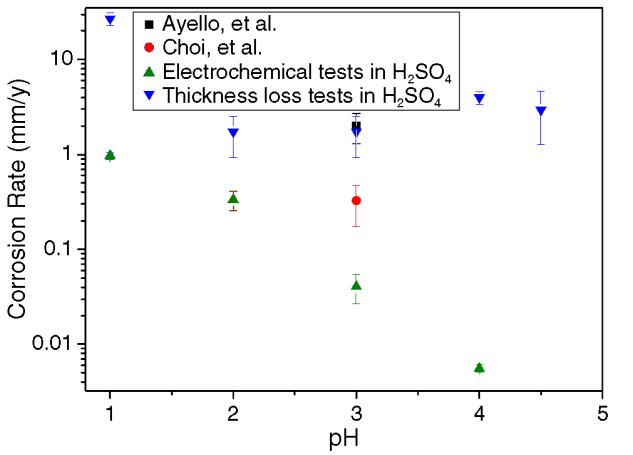

FIGURE 8. *Corrosion rate measurement of steel samples in supercritical CO_2 (Ayello, et al.,[10] and Choi, et al.[18]) vs. in H_2SO_4.*

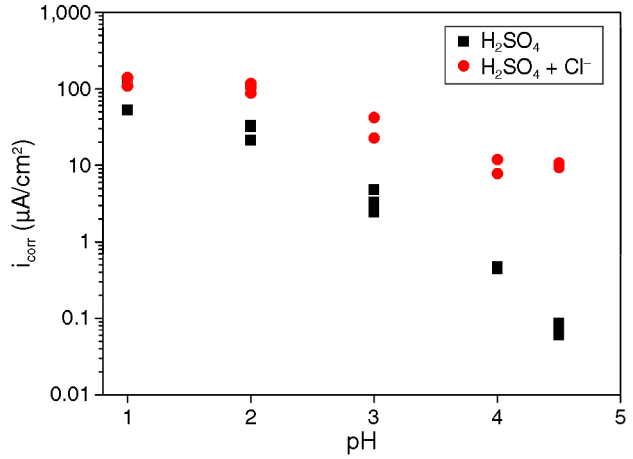

FIGURE 9. *i_{corr} vs. pH from polarization curves collected for steel samples in H_2SO_4 and H_2SO_4 + 0.6 M NaCl electrolytes at 25°C.*

The ability to be able to replicate electrochemical data for H_2CO_3 electrolytes using H_2SO_4 (as in Figure 6) is important, since it means a much wider pH range (and much better control of test pH) can be achieved to study mechanistic aspects and electrode kinetics in a laboratory setting. As previously mentioned, H_2CO_3 can only be produced in-solution and is, hence, very difficult to work with; higher concentrations can only be achieved under high pressure (in which instances of large matrices of polarization tests are difficult to obtain).

This is experimentally shown in Figure 8, where the corrosion rate of steel in supercritical CO_2 from two other authors was plotted against results obtained from steel samples immersed in H_2SO_4.

From Figure 8, it can be seen that corrosion rate results obtained from steel samples in H_2SO_4 is not too dissimilar with those in supercritical CO_2—both from electrochemical and thickness loss measurements (the latter is discussed further below, but presented here for completeness). The supercritical CO_2 tests run by both authors are focused around pH ~3, as a result of a pressure threshold that limits pH to ~3, from which point onward is not experimentally or practically feasible. The similarity in corrosion rates gives merit to the hypothesis that the corrosive property of supercritical CO_2 is attributed to the high acidity of H_2CO_3 formed in situ. A higher corrosion rate can be seen from experiments run by Ayello, et al.,[10] which is possibly because of the higher pressures used (75.8 bar compared to 50 bar by Choi and Nešić[18]). We also note that Ayello has performed tests in the presence of impurities; however, these were not included in Figure 8 since we are looking at the role of a single (H_2CO_3) acid to compare with in Figure 8.

Response in Sulfuric Acid + 0.6 M Sodium Chloride (NaCl) — The corrosion rate measured in H_2SO_4 solution with and without 0.6 M NaCl additions is seen in Figure 9.

As previously shown, the characteristic decrease in the rate of corrosion with increasing pH is observed; however, there is an incremental increase in the i_{corr} measured in the presence of 0.6 M NaCl, with the increment being more obvious as pH increased. If chemical modeling is carried out (via the use of MEDUSA[†,25] shown in Figure 10) as a function of concentration vs. pH for H_2SO_4 + 0.6 M Cl^-, it can be seen that the concentration of H_2SO_4 starts to decrease below pH ~1, and reaches a minimum value near pH ~4, while there is no species formed in situ that contain or bind Cl^-. Consequently, the Cl^- is free to enhance corrosion.

It is noted that there is an increase in corrosion rate with 0.6 M NaCl impurities, although it is more evident above pH 4. According to Masamura, et al.,[26] the corrosion rate of carbon steel is affected only slightly by NaCl content up to 10% at 150°C and 5.5 MPa. However, at 20% NaCl, a corrosion rate of 17 mm/y was reported. This is because of carbonic

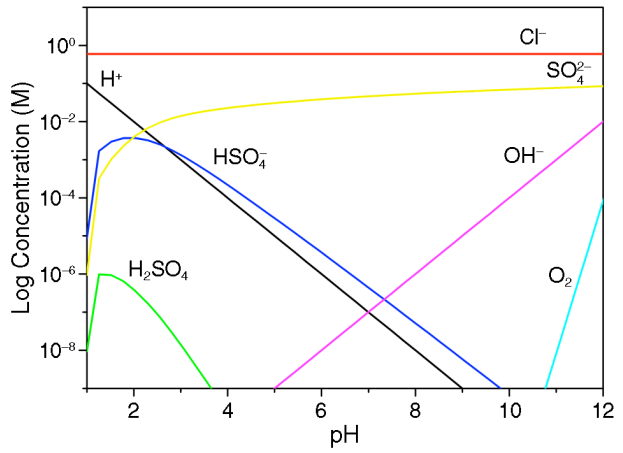

FIGURE 10. *Log concentration (in M) vs. pH of a H_2SO_4 + 0.6 M Cl^- system as calculated via chemical modeling simulation.[25]*

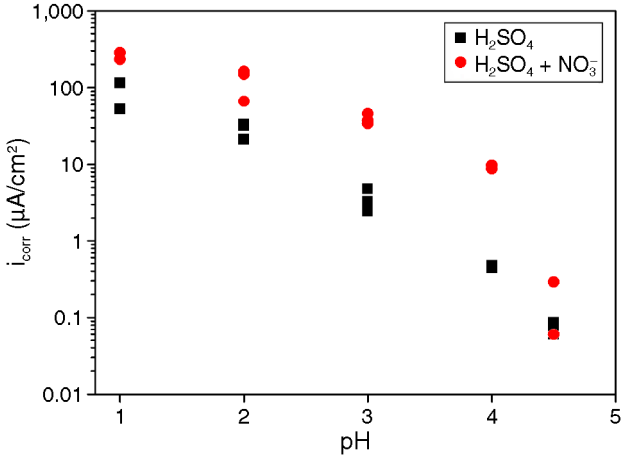

FIGURE 11. *i_{corr} vs. pH from polarization curves collected for steel samples in H_2SO_4 and H_2SO_4 + 0.6 M $NaNO^3$ electrolytes at 25°C.*

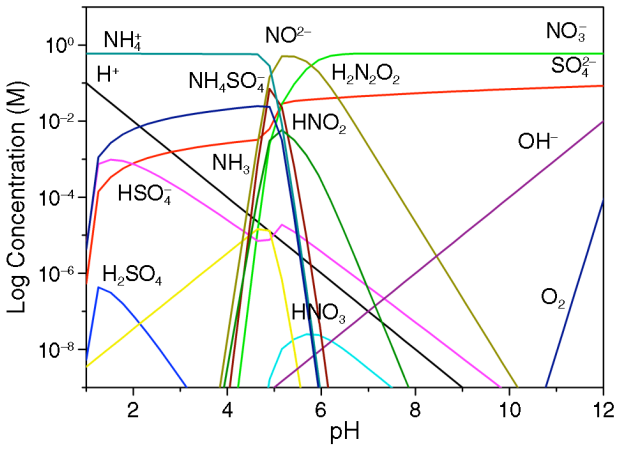

FIGURE 12. *Log concentration (in M) vs. pH of a H_2SO_4 + 0.6 M NO_3^- system as calculated via chemical modeling simulation.[25]*

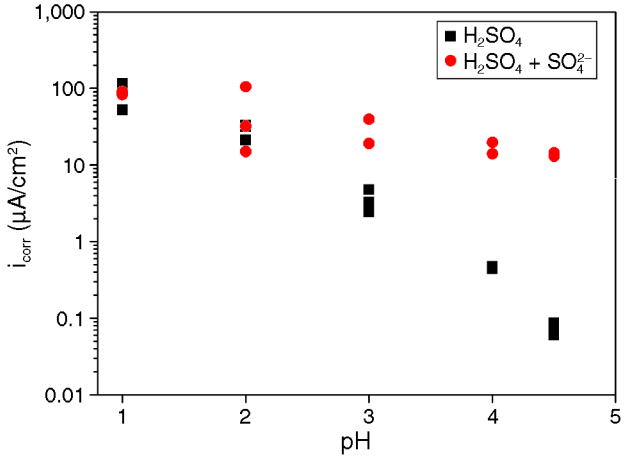

FIGURE 13. *i_{corr} vs. pH from polarization curves collected for steel samples in H_2SO_4 and H_2SO_4 + 0.6 M Na_2SO_4 electrolytes at 25°C.*

substances that accelerate corrosion of carbon steel through their cathodic reactions on the steel surface in the low pH region.

Response in Sulfuric Acid + 0.6 M $NaNO_3$ — The abridged corrosion results from the tests in H_2SO_4 + 0.6 M $NaNO_3$ are given in Figure 11.

Electrochemical results show that $NaNO_3$ impurities tend to increase corrosion rates when added to an acidic environment. However, corrosion rates show a steep decline from pH 4.5 onward, unlike results seen with Cl^- impurities, where corrosion rates stabilized at pH 4.

In Figure 12, it can be seen that a system consisting of NO_3^- impurities is more complex than a H_2SO_4 + Cl^- system. Chemical modeling[25] simulation showed that the amount of species formed in situ is two times that of a H_2SO_4 + Cl^- system.

In particular, HNO_3 is formed in this system (in situ), possibly lowering the pH in solution even further (a test intended for pH 3 could be at a lower pH), which could explain the relatively higher corrosion rates observed in the presence of 0.6 M $NaNO_3$. Among all the impurities (and tests), the corrosion rate including NO_3^- impurities was the highest. A review of the literature indicated that Samiea, et al.,[27] perhaps also have observed synergy between HNO_3 and sulfur-containing solutions.

Response in Sulfuric Acid + 0.6 M Sodium Sulfate (Na_2SO_4) — The third potential impurity tested was the addition of additional SO_4^{2-} ions in H_2SO_4, thus increasing the H_2SO_4 concentration overall. In Figure 13, a similar trend is observed in which impurities showed higher corrosion rates. However, this was only observed from pH 3 onward, where pH 1 to 2 showed minimal difference despite the increased H_2SO_4 concentration.

Figure 14 shows the corresponding system via chemical modeling simulation. In comparison to Figure 10, results in pure H_2SO_4 showed a maximum log concentration of 10^{-6} M at pH 1, while the increased

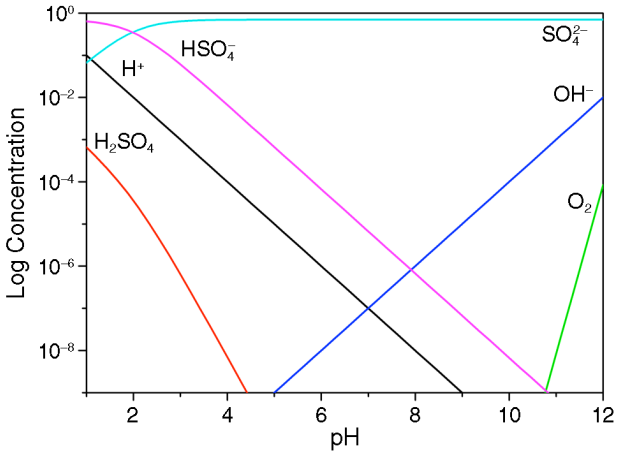

FIGURE 14. *Log concentration (in M) vs. pH of a H_2SO_4 + 0.6 M SO_4^{2-} system as calculated via chemical modeling simulation.[25]*

concentration of H_2SO_4 in Figure 14 showed that a similar concentration was achieved at a pH as high as 3. This could explain why the graph showed steady corrosion rates after pH 3 with SO_4^{2-} impurities, while pure H_2SO_4 continued to decrease in terms of corrosion rate.

According to Choi, et al.,[16] addition of 1% SO_2 in supercritical CO_2 dramatically increased corrosion rates of carbon steel. Corrosion products on the surface were identified via Raman spectroscopy to contain iron, sulfur, and oxygen. It is hypothesized that the formation and reaction of H_2SO_4 with steel is the cause of high corrosion rates in their tests.

In general, the effect of Cl^-, NO_3^-, and SO_4^{2-} impurities in acidic environments have been proven detrimental (in terms of measured i_{corr} values and chemical modeling simulation[25]) to steel. Through chemical modeling simulation[25] simulation, it was discovered that Cl^- does not bind to any species formed in H_2SO_4, leaving it free to increase corrosion rates as expected for steel corrosion. In contrast, the addition of sodium nitrate ($NaNO_3$) showed a more complex system in chemical modeling simulation,[25] and increased corrosion was attributed to the synergistic effect between NO_3^- and acidic solutions. On the other hand, the addition of SO_4^{2-} to H_2SO_4 further increased the acidity of the electrolyte, thus enhancing corrosion.

Weight and Thickness Loss Test Results

Long-term immersion tests were initially conducted in H_2SO_4 electrolytes that were adjusted to be between pH 1 and 5, followed by repeat tests with added impurities (Cl^-, NO_3^-, SO_4^{2-}). The weight and thickness loss results are shown in Figures 15 and 16, respectively.

It can be seen that weight loss follows a log-linear decreasing pattern with increasing pH, where solutions containing impurities show higher corrosion rates. It is also noted that the two measures, weight and thickness loss, seem to show the same trend. Both graphs show a significant amount of weight and thickness loss in pH 1 solutions, and more stable and lower rates from pH 2 onward.

A similar analysis can be applied to results with NO_3^- and SO_4^{2-} impurities. The highest corrosion rate (weight and thickness loss) is recorded in pH 1 solutions, followed by significantly reduced rates. In general, solutions with impurities showed higher corrosion rates compared to H_2SO_4 alone.

Out of all the impurities, the addition of 0.6 M NaCl resulted in the highest corrosion rates in terms of weight and thickness loss, followed by an equal amount in 0.6 M $NaNO_3$ and 0.6 M Na_2SO_4, and finally lowest in pure H_2SO_4. Although the addition of SO_4^{2-} impurities does not significantly alter weight loss, thickness loss results in Figure 16 showed improved rates over pure H_2SO_4 from pH 2 onward.

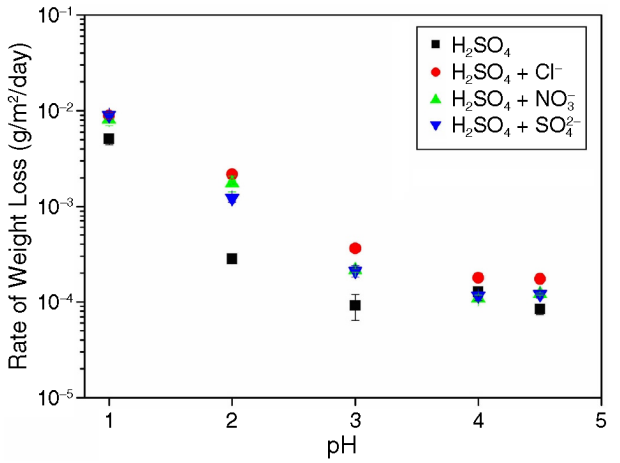

FIGURE 15. *Rate of weight-loss vs. pH data of steel samples immersed in H_2SO_4, H_2SO_4 + 0.6 M NaCl, H_2SO_4 + 0.6 M $NaNO_3$, and H_2SO_4 + 0.6 M Na_2SO_4 electrolytes at 25°C.*

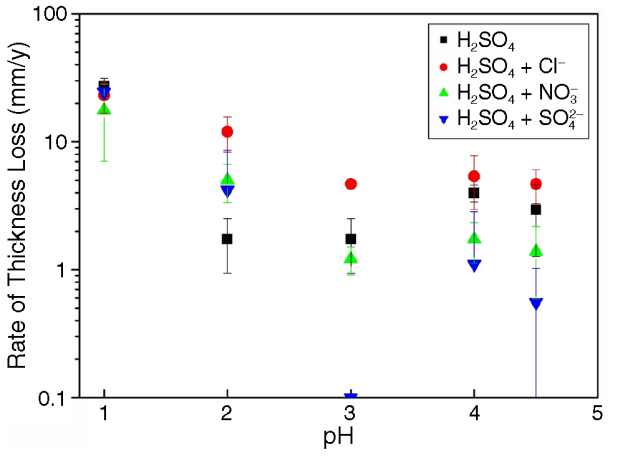

FIGURE 16. *Rate of thickness loss vs. pH data of steel samples immersed in H_2SO_4, H_2SO_4 + 0.6 M NaCl, H_2SO_4 + 0.6 M $NaNO_3$, and H_2SO_4 + 0.6 M Na_2SO_4 electrolytes at 25°C.*

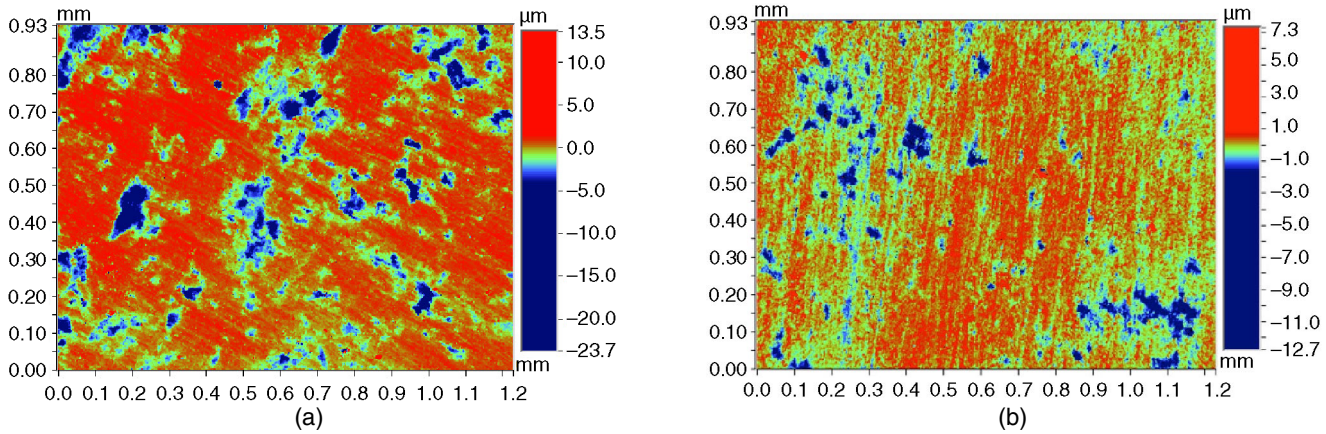

FIGURE 17. *Optical profilometry image of steel samples immersed in (a) pH 2 H_2SO_4 at 25°C and (b) pH 4.5 H_2SO_4 at 25°C.*

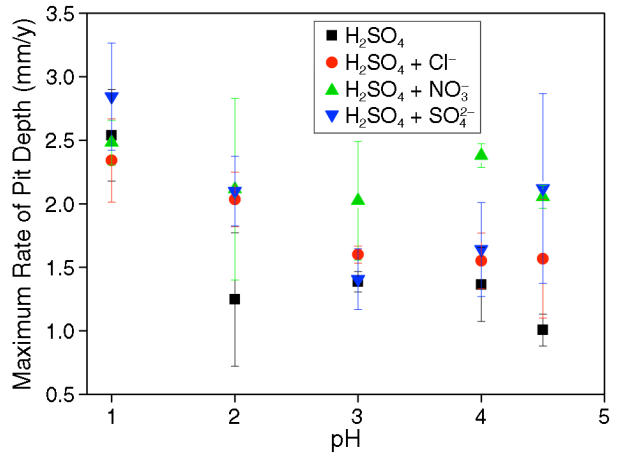

FIGURE 18. *Maximum rate of pit depth of steel samples in H_2SO_4, H_2SO_4 with 0.6 M NaCl, 0.6 M $NaNO_3$, and 0.6 M Na_2SO_4 at 25°C.*

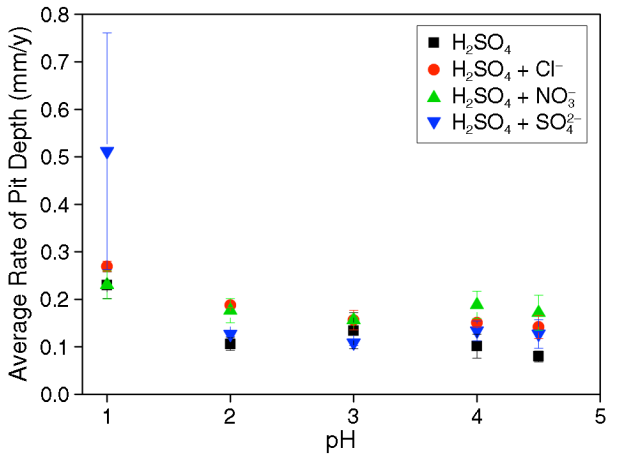

FIGURE 19. *Average rate of pit depth of steel samples in H_2SO_4, H_2SO_4 with 0.6 M NaCl, 0.6 M $NaNO_3$, and 0.6 M Na_2SO_4 at 25°C.*

Profilometry Results

Following exposure tests to characterize the nature and extent of corrosion evolved in acidic electrolytes, data was collected using optical profilometry (OP). The reason for this was to assess if the corrosion morphology was uniform or localized, and to what extent any localization would occur. This has direct relevance to pipeline systems where the management of corrosion differs significantly when corrosion is non-uniform and local rates of attack can be large. Sample OP images are seen in Figure 17, and abridged presentation of OP data is given in Figures 18 and 19.

From Figure 17, it is evident that the form of attack observed did indeed take the form of localized corrosion, and pitting was observed. This is revealed by the valleys in the OP images, with concomitant uniform corrosion throughout. Figure 17 shows that an increase in pH from 2 to 4.5 decreases pit density and maximum pit depth (–23.7 µm to –12.7 µm), indicating that there is a relationship between pit activity and acid strength (i.e., pH).

Image analysis yields the pitting relevant parameters in Figure 18 (maximum rate of pit depth) and Figure 19 (average rate of pit depth) in mm/y.

In general, the graphs show minimal difference in average pit depth across all pH ranges. However, maximum pit depth (Figure 18) across all experiments revealed depths measured to exceed a localized corrosion rate of 2.5 mm/y, signifying extensive pitting corrosion may occur during these simulated conditions that are typical of CO_2 corrosion. A common pattern for all experiments showed the highest damage in pH 1 solutions, followed by decreased depths from pH 2 onward.

Experimental tests show that the critical chloride concentration to initiate pitting in Type 304 (UNS S30400)[(1)] stainless steel is 10^{-3} M,[28] which indicates that localized corrosion occurred during the tests with Cl^- impurities (>1 M). In a separate test, it is shown that Cl^- ions tend to increase the chances of passive film breakdown (rather than inhibit surface repassivation).[29]

[(1)] UNS numbers are listed in *Metals and Alloys in the Unified Numbering System*, published by the Society of Automotive Engineers (SAE International) and cosponsored by ASTM International.

OP data for H_2SO_4 in $NaNO_3$ is not too dissimilar to the rest of the OP results, although it is widely known that nitrates are a common corrosion inhibitor. This is probably because of the co-speciation of acids, with nitric acid (HNO_3) seen in Figure 12. Experimental tests have shown that although HNO_3 increases pitting potential, it is susceptible to crevice corrosion in water-containing impurities.[30]

The highest amount of pitting was found in H_2SO_4 with 0.6 M Na_2SO_4 impurities, where a maximum pit depth rate of 3.26 mm/y was recorded.

General Discussion

The area of CO_2 pipeline corrosion is a topic that will emerge at the forefront of technical challenges in the coming years. As a fundamental approach, small amounts of H_2CO_3 and H_2SO_4 acids were used in experimental tests with a selection of impurities at fixed concentrations. Ultimately, a threshold limit in terms of the concentration of all the components likely to be in the CO_2 pipe stream will need to be quantified before any confidence or national standards in CO_2 pipelines can exist.

The elementary tests herein have shown the issues that can arise in supercritical CO_2 corrosion by way of simple tests in aqueous electrolytes. It is observed that corrosion is pH- and acid strength-driven, and that impurities can permit the co-speciation of additional acids that further lower pH. Corrosion rates were shown to increase logarithmically as pH decreased linearly. We revealed that tests in simulated environments give merit for benchmarking and show the wider range of rates that can be expected. In all cases, impurities increased the rate of corrosion, including thickness and weight loss. Corrosion was found be localized in nature, in spite of low bulk pH. We observed that the ensuing extent of corrosion is very rapid (i.e., mm/y) in many cases and if this work is benchmarked with supercritical CO_2 tests, then a holistic framework for corrosion damage accumulation assessment can be revealed. This is essential in the assessment of CCS technology.

CONCLUSIONS

Experiments in aqueous electrolytes containing H_2CO_3, H_2SO_4, and impurities likely to be present in CCS streams were investigated. This will begin to build a simple knowledge base of information that may be useful in simulating supercritical CO_2 corrosion. The impurities investigated were H_2SO_4, Cl^-, NO_3^-, and SO_4^{2-}. Results from electrochemical, weight and thickness loss, and profilometry tests show the following:

❖ Corrosion kinetics in the presence of H_2CO_3 are pH-driven.

❖ Carbonic acid (and H_2SO_4) corrosion is under anodic control. As pH is lowered, the measured corrosion rates increase logarithmically.

❖ Carbonic acid is 100 times less corrosive compared to H_2SO_4 on a concentration basis, which is expected since H_2CO_3 is a weak acid. NO_3^- impurities show the highest impact on corrosion rates among all tests conducted.

❖ Weight and thickness loss tests revealed that severe corrosion occurs in highly acidic solutions. The difference between pH 1 and pH 2 is about 10 to 15 times. This shows rather starkly that co-speciation of acids in the presence of impurities (which can lead to a decrease in pH) can be very detrimental in terms of corrosion.

❖ Weight and thickness loss tests revealed that solutions with impurities show relatively stable corrosion rates across a pH range of 1 to 5, similarly having highest rates in pH 1 solutions.

❖ Optical profilometry results suggest that extensive pitting occurs during H_2CO_3/acid corrosion, with all tests exceeding a maximum pitting corrosion rate of 2.5 mm/y.

ACKNOWLEDGMENTS

S. Sim is supported by an MGS scholarship from Monash University.

REFERENCES

1. D. Zheng, D. Che, Y. Liu, *Corros. Sci.* 50 (2008): p. 3005-3020.
2. F. Yu, K.W. Gao, Y.J. Su, J.X. Li, L.J. Qiao, W.Y. Chu, M.X. Lu, *Mater. Lett.* 59 (2005): p. 1709-1713.
3. F.M. Song, *Electrochim. Acta* 55 (2010): p. 689-700.
4. X. Hu, A. Neville, *Wear* 267 (2009): p. 2027-2032.
5. I.S. Cole, P. Corrigan, S. Sim, N. Birbilis, *Int. J. Greenhouse Gas Control* 5, 4 (2011): p. 749-756.
6. J. Gibbins, "Carbon Capture and Storage: A State-of-the-Art Overview," The First International Forum on the Transportation of CO_2 by Pipeline, held July 1-2 (London, U.K.: The Carbon Capture & Storage Association [CCSA], 2010), p. 10.
7. A. Goodman, A. Hakala, G. Bromhal, D. Deel, T. Rodosta, S. Frailey, M. Small, D. Allen, V. Romanov, J. Fazio, N. Huerta, D. McIntyre, B. Kutchko, G. Guthrie, *Int. J. Greenhouse Gas Control* 5, 4 (2011): p. 952-965.
8. J. Gale, J. Davison, *Energy* 29, 9-10 (2004): p. 1319-1328.
9. H. Kruse, M. Tekiela, *Energy Convers. Manage.* 37, 6-8 (1996): p. 1013-1018.
10. F. Ayello, N. Sridhar, K. Evans, R. Thodla, "Effect of Liquid Impurities on Corrosion of Carbon Steel in Supercritical CO_2," Proc. 8th Int. Pipeline Conf. (New York, NY: ASME, 2010).
11. F. Eldevik, B. Graver, L.E. Torbergsen, O.T. Saugerud, *Energy Procedia* 1, 1 (2009): p. 1579-1585.
12. F. Ayello, K. Evans, R. Thodla, N. Sridhar, "Effect of Impurities on Corrosion of Steel in Supercritical CO_2," CORROSION/2010, paper no. 10193 (Houston, TX: NACE, 2010).
13. M. Maroto-Valer, *Developments and Innovation in Carbon Dioxide (CO_2) Capture and Storage Technology* (Oxford, Cambridge, New Delhi: Woodhead Publishing Limited, 2010), p. 411-412.
14. A. Kather, S. Kownatzki, *Int. J. Greenhouse Gas Control* 5, Supplement 1 (2011): p. S204-S209.
15. B.P. McGrail, H.T. Schaef, V.A. Glezakou, L.X. Dang, A.T. Owen, *Energy Procedia* 1, 1 (2009): p. 3415-3419.
16. Y.-S. Choi, S. Nešić, D. Young, *Environ. Sci. Technol.* 44 (2010): p. 9233-9238.
17. E.M. Russick, G.A. Poulter, C.L.J. Adkins, N.R. Sorensen, *J. Supercrit. Fluids* 9, 1 (1996): p. 43-50.
18. Y.-S. Choi, S. Nešić, *Int. J. Greenhouse Gas Control* 5, 4 (2011): p. 788-797.
19. R. Marshall, "OLI Simulation Studies," http://www.olisystems.com/oliengine.htm, November 25, 2010.

20. F. Eldevik, B. Graver, L.E. Torbergsen, O.T. Saugerud, *Energy Procedia* 1, 1 (2009): p. 1579-1585.
21. T. Wall, R. Stanger, Y. Liu, "Gas Cleaning Challenges for Coal-Fired Oxy-Fuel Technology with Carbon Capture and Storage," *Fuel* (2011), in press, corrected proof.
22. J. Wang, D. Ryan, E.J. Anthony, N. Wildgust, T. Aiken, *Energy Procedia* 4 (2011): p. 3071-3078.
23. H. Li, J. Yan, M. Anheden, *Appl. Energy* 86, 2 (2009): p. 202-213.
24. E.J. Granite, T. O'Brien, *Fuel Process. Technol.* 86, 14-15 (2005): p. 1423-1434.
25. P. Ignasi, "Chemical Equilibrium Diagrams," http://www.kemi.kth.se/medusa/, November 23, 2010.
26. K. Masamura, S. Hashizume, K. Nunomura, J.-I. Sakai, I. Matsushima, *Adv. CO_2 Corros.* 1 (1984): p. 143-150.
27. F. Samiea, J. Tidblad, V. Kucera, C. Leygraf, *Atmos. Environ.* 41 (2007): p. 4888-4896.
28. E.A. Abd El Meguid, N.A. Mahmoud, S.S. Abd El Rehim, *Mater. Chem. Phys.* 63, 1 (2000): p. 67-74.
29. Y.F. Cheng, M. Wilmott, J.L. Luo, *Appl. Surf. Sci.* 152, 3-4 (1999): p. 161-168.
30. M.A. Barbosa, *Corros. Sci.* 23, 12 (1983): p. 1293-1305.